Muons as a probe of magnetism in molecule-based low dimensional magnets

2004 J. Phys.: Condens. Matter 16 S4563

(http://iopscience.iop.org/0953-8984/16/40/009)

INSTITUTE OF PHYSICS PUBLISHING JOURNAL OF PHYSICS: CONDENSED MATTER

J. Phys.: Condens. Matter **16** (2004) S4563–S4582 PII: S0953-8984(04)75384-9

Muons as a probe of magnetism in molecule-based low dimensional magnets

Tom Lancaster[1], Stephen J Blundell[1], Francis L Pratt[2], Michael L Brooks[1], Jamie L Manson[3], Euan K Brechin[4], Cyril Cadiou[4], David Low[4], Eric J L McInnes[4] and Richard E P Winpenny[4]

[1] Department of Physics, Clarendon Laboratory, Oxford University, Parks Road, Oxford OX1 3PU, UK
[2] ISIS Facility, Rutherford Appleton Laboratory, Chilton, Oxfordshire OX11 0QX, UK
[3] Department of Chemistry and Biochemistry, Eastern Washington University, Cheney, WA 99004, USA
[4] Department of Chemistry, The University of Manchester, Oxford Road, Manchester M13 9PL, UK

E-mail: t.lancaster@physics.ox.ac.uk, s.blundell@physics.ox.ac.uk and f.pratt@rl.ac.uk

Received 26 January 2004
Published 24 September 2004
Online at stacks.iop.org/JPhysCM/16/S4563
doi:10.1088/0953-8984/16/40/009

Abstract

We present the results of muon spin relaxation (μ^+SR) studies on low dimensional molecular magnet systems. μ^+SR measurements have been carried out on the Cu-based chain compounds $CuX_2(pyz)$ (where X = Br, Cl, NCS and pyz = pyrazine) as a function of temperature and applied longitudinal magnetic field. Oscillations in the time dependence of the muon polarization, characteristic of magnetic order at two distinct muon sites, are detected in both $CuBr_2(pyz)$ (below $T_N = 3.6(1)$ K) and $CuCl_2(pyz)$ (below $T_N = 3.2(2)$ K). No evidence of magnetic order is observed in $Cu(NCS)_2(pyz)$ down to 0.35 K. The results are discussed in terms of the estimated Cu–X–Cu and Cu–(pyz)–Cu exchange constants. The theory of μ^+SR in high spin molecule (HSM) systems, which are effectively zero-dimensional magnets, is discussed and results are presented on $[Ni_{12}(chp)_{12}(O_2CMe)_{12}(H_2O)_6(THF)_6]$ ($S = 12$), $[Mn_9O_7(OAc)_{11}(thme)(py)_3(H_2O)_2]$ ($S = 17/2$) and $[Fe_{14}(bta)_6(O)_6(OMe)_{18}Cl_6]$ ($S \geqslant 23$). Measurements made in applied longitudinal magnetic fields on HSM materials at dilution refrigerator temperatures strongly suggest that dynamic local magnetic field fluctuations are responsible for the relaxation of the muon spin ensemble. Trends in temperature and field dependent behaviour in these systems, as probed by the muon, are discussed.

(Some figures in this article are in colour only in the electronic version)

1. Introduction

Muon spin relaxation (μ^+SR) has been extensively used in the study of various organic and molecular magnets (for a review, see [1]). Muons are a *local* probe of internal fields, and therefore can be used to follow an order parameter as a function of temperature. Muons sensitively probe very weak magnetism sometimes found in heavy fermion systems [2] and therefore are demonstrably suitable for studying low moment magnetism. In multiphase samples, muons give signals proportional to the volume fraction of each phase, so they can be used to distinguish between a sample which is uniformly weakly magnetic and one which is non-magnetic but contains a tiny fraction of strongly magnetic impurity. This can be helpful in validating claims of authentic molecular magnets. The technique works very well in zero applied magnetic field and at millikelvin temperatures since the incident muons easily pass through dilution refrigerator windows. Muons provide information on organic antiferromagnets [3, 4], spin-gap systems [5] and spin crossover systems [6] as well as on various types of organic ferromagnets [7–10]. If there are a range of muon sites in a particular system, μ^+SR can provide information about internal magnetic field distributions. Studies can also be performed of the magnetic fluctuations and spin dynamics, even above the magnetic transition temperature.

Some of the most exciting developments in molecular magnetism have arisen from using synthetic chemical techniques to engineer structures with low dimensionality. This paper describes μ^+SR experiments which have been performed on two families of low dimensional molecular magnets. The first family is obtained by joining $S = 1/2$ Cu ions by organic ligands such as pyrazine into chains and then assembling these by stacking the chains into sheets bridged by halide ions or thiocyanate ions. These are quasi-one-dimensional antiferromagnets, since the interactions in the chains are much stronger than those between the chains. Nevertheless, the interchain interactions are important in determining whether a particular compound exhibits long range magnetic order. The second family are high spin molecules (HSMs), which are small magnetic clusters and are effectively zero-dimensional magnets. This paper is structured as follows: following a brief description of the experimental details, the results on the family of quasi-one-dimensional antiferromagnets are described in section 3 and those for the single-molecule magnets are described in section 4. The conclusions are presented in section 5.

2. Experimental details

Our experiments were performed on the MuSR and EMU beamlines at the ISIS facility, Rutherford Appleton Laboratory, Didcot, UK, and the πM3 beamline at the Paul Scherrer Institute (PSI), Villigen, Switzerland. In all our experiments positrons are detected by scintillation counters which are positioned in front of and behind the sample with respect to the initial muon momentum direction. The muon spin relaxation function $A(t)$ (also known as the asymmetry) is defined by $A(t) = [N_{\rm B}(t) - \alpha N_{\rm F}(t)]/[N_{\rm B}(t) + \alpha N_{\rm F}(t)]$, where $N_{\rm B}(t)$ and $N_{\rm F}(t)$ represent the number of positron counts in the backward and forward detectors respectively as a function of time and α is an experimental calibration constant which is usually close to unity. The samples were each wrapped in a 25 μm silver foil and mounted on a silver backing plate in a ^{4}He or ^{3}He cryostat or on to the cold finger of a dilution refrigerator. Silver foil is used because it gives a non-relaxing muon signal, and hence only contributes a temperature independent constant to $A(t)$.

3. One dimension: spin-$\frac{1}{2}$ chain compounds

3.1. Copper chain compounds

Exchange interactions mediated by organic ligands can lead to magnetic ordering at high temperatures [11]. Pyrazine (pyz) has been used extensively in this respect [12]. Recently, the

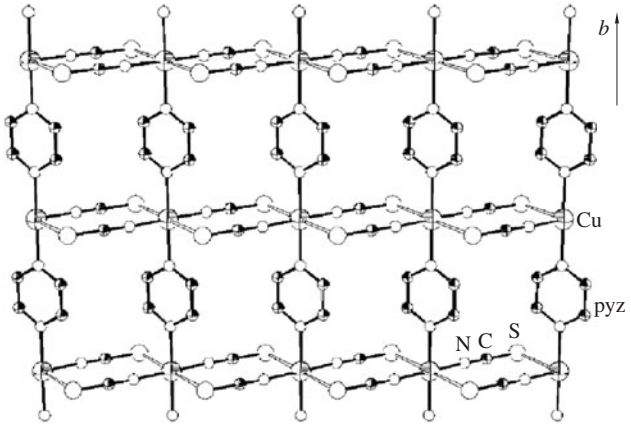

Figure 1. The two-dimensional network structure of $Cu(NCS)_2(pyz)$ showing the cross-linking Cu–pyz–Cu and Cu–NCS–Cu chains [13]. The *b*-axis is shown.

compound $Cu(NCS)_2(pyz)$ was prepared which combines pyz, spin-$\frac{1}{2}$ Cu ions and thiocyanate (NCS^-) anions [13]. The structure consists of parallel chains of Cu^{2+} ions bridged by the bidendate pyz ligands organized along the *b*-axis (see figure 1). Thiocyanate anions lie in the *ac*-plane and bridge the Cu–pyz–Cu chains together to form a two-dimensional rectangular grid. The sheets pack in a staggered fashion so that the Cu ion of one sheet lies above (and below) the centroid of adjacent two-dimensional networks [13]. Neutron scattering measurements on $Cu(NCS)_2(pyz)$ showed no magnetic Bragg reflections down to 4 K. A broad feature observed in the magnetic susceptibility around 7 K fitted well to a one-dimensional Bonner–Fisher uniform antiferromagnetic chain model with $J/k_B = -8.0(1)$ K ($\sim$0.7 meV). Electronic structure calculations suggest that the superexchange interaction along the Cu–(pyz)–Cu chains is $\sim$1500 times stronger than that between chains, mediated by the NCS^- anions [12], making this material a highly successful experimental realization of a one-dimensional Heisenberg antiferromagnet.

Salts with the same structure as $Cu(NCS)_2(pyz)$ may also be synthesized using halide anions instead of (NCS) to bridge the Cu–pyz–Cu chains. As a result, the salts $CuCl_2(pyz)$ and $CuBr_2(pyz)$ have also been prepared. Magnetic susceptibility studies show broad maxima at 17 and 34 K for the Cl^- and Br^- compounds respectively [14]. The data can be partially fitted by a Bonner–Fisher antiferromagnetic chain model but the best fit is obtained by taking into account interchain interactions. Neutron measurements have been performed down to 50 mK on $CuCl_2(pyz)$ and $CuBr_2(pyz)$ but no magnetic Bragg peaks were observed.

In this paper, we report the first μ^+SR measurements made on $CuBr_2(pyz)$, $CuCl_2(pyz)$ and $Cu(NCS)_2(pyz)$ as a function of temperature and applied magnetic field.

3.2. μ^+SR data

3.2.1. $CuBr_2(pyz)$. The sample of $CuBr_2(pyz)$ measured in this study had been deuterated, to form $CuBr_2(pyz\text{-}d_4)$, for the purposes of magnetic neutron diffraction measurements. We do not believe that the deuteration has a significant effect on the magnetism of this material. Zero-field (ZF) and longitudinal field (LF) μ^+SR measurements were made on the powder sample of $CuBr_2(pyz\text{-}d_4)$ on the MuSR beamline at the ISIS facility using a standard orange cryostat [15].

ZF asymmetry spectra are shown in figure 2. Below $T = 3.6(1)$ K, oscillations in the positron asymmetry are clearly observable. These are characteristic of a quasistatic local magnetic field at the muon site, which causes a coherent precession of the spins of those muons with a component of their spin polarization perpendicular to this local field (expected to be 2/3 of the total polarization). The frequency of the oscillations is given by $\nu_i = \gamma_\mu B_i/2\pi$, where γ_μ is the muon gyromagnetic ratio ($\equiv 2\pi \times 135$ MHz T^{-1}) and B_i is the local field at the ith muon site. Any distribution in magnitude of local fields due to spatial (static) or temporal (dynamic) fluctuations will lead to a relaxation of the oscillating signal. Fourier analysis of the measured spectra reveals there to be two separate spin precession frequencies (see *inset:* figure 2): a large, low frequency contribution ν_1 and a broader, low intensity component ν_2 at higher frequency. This suggests the presence of two distinct muon sites in magnetically ordered regions within the crystal below $T = 3.6(1)$ K. As described above, the magnetic susceptibility data for this material are strongly suggestive of antiferromagnetic interactions at low temperatures. We therefore describe the temperature at which the oscillations vanish as the Néel temperature T_N for this material.

The amplitudes of the oscillating components, A_1 and A_2, are found to be in a constant ratio of 4:1 across the measured temperature range. This suggests two distinct muon sites in the crystal, with the site associated with ν_1 being four times more probable than the site associated with ν_2.

Neither of the oscillating components can be fitted with a simple $\cos(2\pi\nu_{1,2}t)$ oscillating functional form. Instead, constant phase offsets $\phi_{1,2}$ are required (nominally $\phi_1 = -64°$ and $\phi_2 = -139°$). This property may possibly be due to an incommensurate component in the magnetic structure of the material or to the delayed formation of the diamagnetic muon species. Alternative parametrizations of the oscillations were considered, including the use of Bessel functions to model incommensurate magnetic order [2, 16], but these resulted in substantially worse fits to the measured spectra.

The data also display a separate relaxing component to the asymmetry. This contribution is characteristic of muons which experience a random distribution of local magnetic fields. At low temperatures this contribution is well described by an exponential function, while close to the transition region it approaches a Gaussian form (figure 2). In order to fit the data over the entire temperature range, we crudely parametrize this behaviour with a stretched exponential function $\exp(-\lambda t)^\beta$. This results in the exponential form of function at short times for $\beta = 1$ and the observed Gaussian form for $\beta = 2$.

The data are best described with the resulting relaxation function:

$$A(t) = A_1\left(\tfrac{1}{3} + \tfrac{2}{3}\exp(-\lambda_1 t)\cos(2\pi\nu_1 t + \phi_1)\right) + A_2\left(\tfrac{1}{3} + \tfrac{2}{3}\exp(-\lambda_2 t)\cos(2\pi\nu_2 t + \phi_2)\right) + A_3\exp(-\lambda_3 t)^\beta + A_{\mathrm{bg}}\exp(-\lambda_{\mathrm{bg}} t), \quad (1)$$

where $\lambda_{1,2,3}$ are relaxation rates. The final term $A_{\mathrm{bg}}\exp(-\lambda_{\mathrm{bg}}t)$ allows for background contributions, such as muons that stop in the sample holder, the cryostat windows or cryostat tail.

The relaxation rate λ_2 is roughly constant at $\lambda_2 = 1.34$ MHz, while λ_1 increases monotonically with increasing temperature from $\lambda_1 = 0.4$ MHz at the lowest measured temperature to $\lambda_1 = 1.2$ MHz as T_N is approached from below.

Figure 3 shows the results of the fitting procedure. The temperature variation of the total amplitude associated with the oscillating component of the relaxation $A_1 + A_2$ and that associated with the relaxing component A_3 are shown in figure 3(a). We find that the relaxing component increases, while the oscillating component decreases, such that the total relaxing asymmetry $A_1 + A_2 + A_3$ remains constant. The oscillatory component suddenly vanishes at $T_N = 3.6(1)$ K.

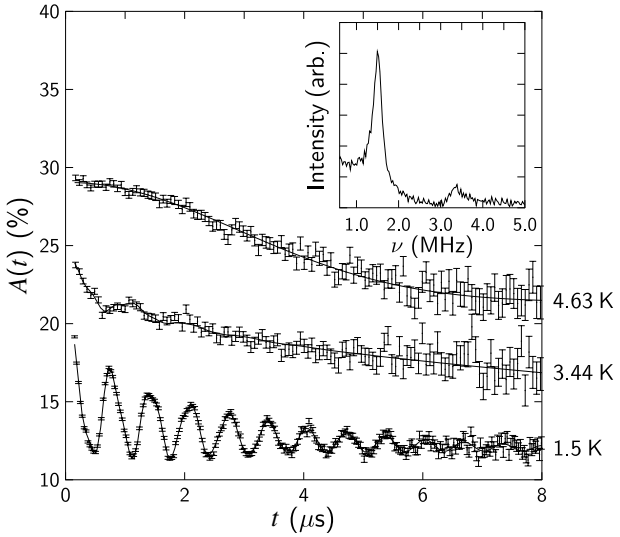

Figure 2. ZF μ^+SR asymmetry spectra for $CuBr_2(pyz\text{-}d_4)$ measured at $T = 1.5$, 3.44 and 4.63 K, showing oscillations below the ordering temperature $T_N = 3.6(1)$ K. For clarity, the data measured at 4.63 K have been offset by +5%. Data measured above T_N tend to a Gaussian form at high temperatures. *Inset:* the Fourier transform of data measured at 1.5 K after subtraction of the non-oscillatory terms, showing two distinct precession frequencies.

Figure 3(b) shows the evolution of the precession frequencies with varying temperature. The frequencies decrease slowly with increasing temperature before their sudden disappearance at T_N. Below T_N, the relaxing component is well described with $\beta = 1$. Above the transition, β increases sharply, saturating at $\beta = 2$ above 5 K as shown in figure 3(c). The associated relaxation rate λ_3 decreases across the entire temperature range, as shown in figure 3(d). We note that the non-relaxing component of the data may be described with alternative fitting schemes and that our approach, using equation (1), is not unique. The results in figures 3(c) and (d) should, therefore, be viewed as a parametrization of the measured spectra.

The application of a longitudinal magnetic field to the sample above T_N causes a decoupling of the relaxing component of the asymmetry at fields below $B = 50$ G (i.e. $\lim_{t\to\infty} A_3(t) = A_3(0)$). At high temperatures, where the ZF spectra are well described by a Gaussian functional form, the B dependent behaviour is consistent with the early time behaviour of a LF Gaussian Kubo–Toyabe (GKT) function (due to a random array of static moments with a Gaussian field distribution [17]). This is most probably due to a static distribution of nuclear magnetic moments, with slow dynamics preventing the recovery of the function at long times. Below T_N, analysis of the field dependence is complicated by considerations of the effect of the applied field on the ordered moments. The observed behaviour is, however, consistent with the quenching of the non-oscillating component below $B \approx 50$ G. This behaviour suggests that the relaxing component is due to a slowly fluctuating or static distribution of magnetic moments across the temperature range. If static, this observed exponential form of the relaxing component may be characteristic of the early time region of a Lorentzian Kubo–Toyabe (LKT) function, due to a random array of static moments with a Lorentzian field distribution [18], although it is hard to see how such a distribution could arise. If instead a dynamic effect is involved, the measured behaviour would imply an upper bound on the relaxation rate ν, namely that $\nu/\gamma_\mu \ll 50$ G (i.e. $\nu \ll 4.3$ MHz). It is interesting to note that relaxation of a similar

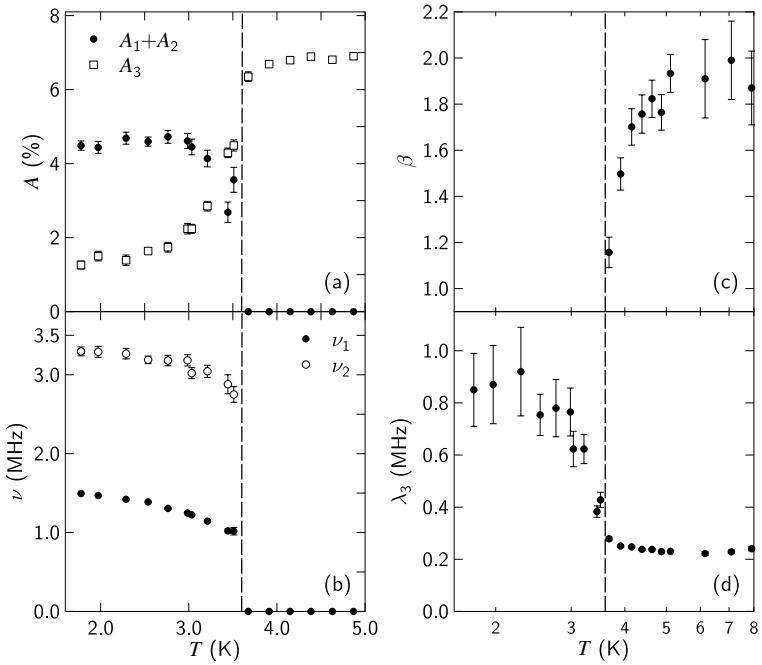

Figure 3. Fitted parameters for measurements made on $CuBr_2(pyz\text{-}d_4)$. (a) The temperature evolution of the asymmetry amplitudes. The sum $A_1 + A_2$ represents the total contribution from the oscillatory terms, while A_3 is due to the stretched exponential term. The broken line shows $T = T_N$. (b) The variation of the two precession frequencies with temperature showing a slow decrease with increasing temperature, up to 3.5 K, above which they are no longer observable. (c) The behaviour of the stretching factor β above T_N. An increase from $\beta = 1$ (exponential relaxation) to $\beta = 2$ (Gaussian relaxation) is observed with increasing temperature. (d) The variation of the relaxation rate λ_3 across the temperature range displaying a decrease as T_N is approached from below.

form was measured in the $S = \frac{1}{2}$ zigzag chain compound $SrCuO_2$ [19] and was attributed to nearly static Lorentzian local fields.

3.2.2. $CuCl_2(pyz)$. Powder samples of $CuCl_2(pyz)$ were measured on the MuSR beamline at the ISIS facility using an orange cryostat. Examples of measured asymmetry spectra are shown in figure 4. Below $T = 3.2(2)$ K, oscillations are observed in the asymmetry at two distinct precession frequencies, from which we conclude that the material magnetically orders below this temperature. Fitting the oscillations again requires the inclusion of phase offsets (in this case $\phi_1 = -67°$ and $\phi_2 = -83°$). As in the case of $CuBr_2(pyz\text{-}d_4)$, magnetic susceptibility measurements motivate us to describe the temperature at which the oscillations vanish as the Néel temperature.

In contrast to the case for $CuBr_2(pyz\text{-}d_4)$, the amplitudes associated with the two precession frequencies, A_1 and A_2, are found to be roughly equal, suggesting that the probability of a muon stopping in either site is roughly the same. A non-oscillatory component is also observed, but makes a larger contribution to the total asymmetry at the lowest temperatures, compared to the case for $CuBr_2(pyz\text{-}d_4)$.

The measured spectra were fitted to equation (1), with λ_1 and λ_2 both fixed at 1.05 MHz. The resulting parameters are shown in figure 5. As in the case of $CuBr_2(pyz\text{-}d_4)$, the amplitudes associated with the relaxing component of the asymmetry A_3 increase with increasing

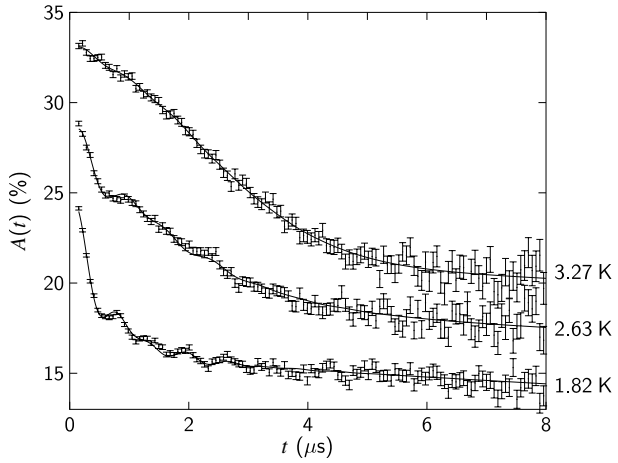

Figure 4. ZF μ^+SR spectra for $CuCl_2$(pyz) measured at $T = 1.818$, 2.63 and 3.27 K. For clarity, data measured at 2.63 K have been offset by +4%, while those measured for 3.27 K has been offset by +8%. Oscillations at two distinct frequencies are observed below the magnetic ordering temperature T_N. The spectra tend to a Gaussian form at high temperatures.

temperature, with a corresponding decrease of the oscillating fraction $A_1 + A_2$ (figure 5(a)). The precession frequencies ν_1 and ν_2 slowly decrease with increasing temperature, before their sudden disappearance (figure 5(b)) at $T_N = 3.2(2)$ K. In contrast to the case for $CuBr_2$(pyz), the stretching factor β begins to increase at a temperature where there is still an appreciable oscillating component. The evolution from $\beta = 1$ to 2 is shown in figure 5(c). The relaxation rate λ_3 (figure 5(d)) decreases smoothly across the entire temperature range.

The application of external fields results in very similar behaviour to that reported for $CuBr_2$(pyz-d_4). The high temperature signal is decoupled by $B = 50$ G suggesting static relaxation, probably due to nuclear moments. Below T_N, the relaxing component is quenched below $B \approx 50$ G.

We conclude that the general trends in behaviour observed in $CuCl_2$(pyz) are similar to those observed in $CuBr_2$(pyz-d_4), namely, the existence of a magnetically ordered phase below $T_N = 3.2(2)$ K in which there are two distinct muon stopping sites (in this case of roughly equal probability). The observed behaviour is very probably attributable to the same mechanisms as occur in $CuBr_2$(pyz-d_4).

3.2.3. Cu(NCS)$_2$(pyz). ZF and LF measurements were made on powder samples of $Cu(NCS)_2$(pyz) on both the MuSR and EMU beamlines at ISIS using a standard orange cryostat and sorption cryostat. No signature of magnetic ordering is observed down to the lowest temperatures obtainable using the sorption cryostat ($T = 0.35$ K). An example spectrum measured at 0.35 K is shown in figure 6. The Gaussian form of the relaxation is very similar to that observed in the high temperature regime for both $CuBr_2$(pyz) and $CuCl_2$(pyz). The application of longitudinal magnetic fields decouples the muon relaxation below $B = 50$ G, confirming the static nature of the field distribution.

We conclude that no magnetic order is detectable down to $T = 0.35$ K in this material. The muon polarization is relaxed by a random, static distribution of internal fields, most likely due to nuclear magnetic moments.

3.2.4. Discussion. The oscillations in the asymmetry for both $CuBr_2$(pyz-d_4) ($T_N = 3.6(1)$ K) and $CuCl_2$(pyz) ($T_N = 3.2(2)$ K) provide clear evidence for long range magnetic

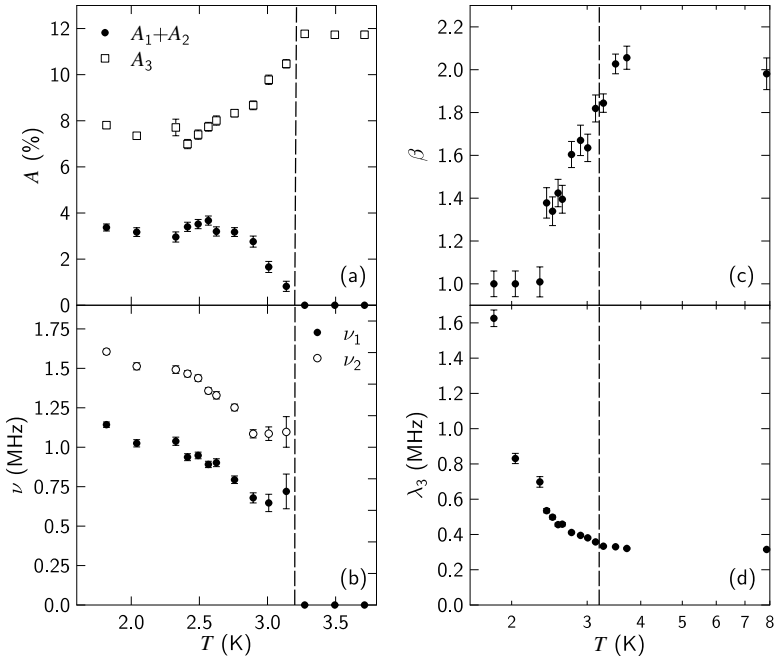

Figure 5. Fitted parameters for measurements made on $CuCl_2$(pyz). (a) The temperature evolution of amplitudes $A_1 + A_2$ (due to the contribution of the oscillatory terms) and A_3 (due to the stretched exponential term). The broken line shows $T = T_N$. (b) The behaviour of the two frequencies precession frequencies as a function of temperature. (c) The temperature evolution of the stretching factor β, across the temperature range. The increase from $\beta = 1$ is seen to start to occur at $T < T_N$. (d) The relaxation rate λ_3 as a function of temperature showing a smooth decrease with increasing temperature.

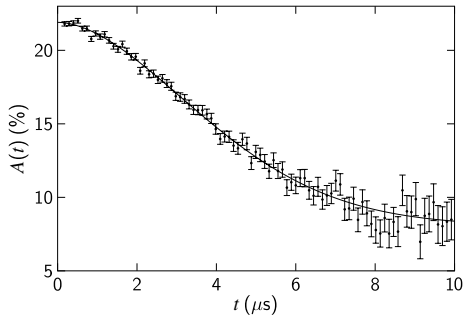

Figure 6. The asymmetry time spectrum for Cu(NCS)$_2$(pyz) measured at $T = 0.35$ K. No oscillations are observed down to this temperature.

order (LRO) in both of these materials for the first time. In contrast, Cu(NCS)$_2$(pyz) shows no evidence of LRO down to 0.35 K. Although the magnetic transitions in $CuBr_2$(pyz-d_4) (figure 3(b)) and $CuCl_2$(pyz) (figure 5(b)) appear discontinuous, the increasing amplitudes of the relaxing components may obscure more gradual changes in frequency. Thermodynamic measurements are required to determine the nature of the phase transition.

The rectangular structure of CuX_2(pyz) as described in section 1 suggests two probable sets of copper superexchange pathways, Cu–(pyz)–Cu and Cu–X–Cu. The material will

show one-dimensional magnetic properties if the exchange constant associated with one of the exchange pathways is significantly larger than the other. Although an ideal one-dimensional antiferromagnetic Heisenberg chain will not show LRO at any temperature, magnetic ordering is possible at temperatures low enough that the interchain exchange interaction $J_\perp$ is comparable with $k_B T$. The antiferromagnetic interchain exchange constant $J_\perp$ may be estimated from the ordering temperature T_N extracted from our data using an expression derived from chain mean-field theory [20], namely

$$|J_\perp| = \frac{T_N}{1.28\left(\ln\left(\frac{5.8J_1}{T_N}\right)\right)^{\frac{1}{2}}}. \tag{2}$$

Here J_1 is the intrachain exchange constant, which may be estimated [21] from the temperature T_M corresponding to the maximum in the measured magnetic susceptibility data for these compounds [14], using the relation

$$T_M \approx 1.282 J_1. \tag{3}$$

This approach yields $J_1 \approx -24.3$ K, $|J_\perp| \approx 1.5$ K for $CuBr_2(pyz\text{-}d_4)$ and $J_1 \approx -13.6$ K, $|J_\perp| \approx 1.4$ K for $CuCl_2(pyz)$. This is suggestive of large, unequal intrachain exchange constants J_1 along the Cu–X–Cu chains and smaller, comparable exchange constants $J_\perp$ along the Cu–(pyz)–Cu chains. We also note that $J_1 \approx -13.6$ K is similar to the value measured for $CuCl_2(py)$ [22] where J_1 ($= -13.4(2)$ K) is also thought to be along the Cu–Cl–Cu chains.

In contrast, the dominant exchange J_1 in the case of $Cu(NCS)_2$ is likely to be along the Cu–(pyz)–Cu chains [13, 12]. Applying the same approach as described above yields $J_1 \approx -5.5$ K for the Cu–pyz–Cu chains and $|J_\perp| < 0.13$ K. As in the well known case of copper pyrazine dinitrate $Cu(pyz)(NO_3)_2$ [23], $Cu(NCS)_2$ presents itself as a good example of a nearly ideal one-dimensional Heisenberg antiferromagnetic chain.

The cause of the relaxing signal in $CuBr_2(pyz\text{-}d_4)$ and $CuCl_2(pyz)$ and its temperature and field dependent behaviour are unclear. It is possibly related to longitudinal relaxation effects within the ordered phase, not accounted for in the model used above. Another possibility is that it is related to muon sites within the sample where the average local field due to the magnetic order either vanishes or is very small. There is also the interesting possibility of behaviour resulting from a paramagnetic muon state in the crystal inducing a perturbation in the system, as was proposed in the case of dichlorobis (pyridine) copper(II) [24]. Transverse field (TF) μ^+SR measurements on these compounds may shed some light on this issue, and we plan to attempt these in the future.

4. Zero dimension: single-molecule magnets

4.1. Single-molecule magnets

High spin molecules (HSMs) are formed from networks of magnetic ions which couple ferromagnetically or antiferromagnetically in such a way as to make the total spin S of the molecule large. These molecules form crystals in which the intermolecular magnetic interactions are small in many cases and may therefore be neglected. HSMs, therefore, act as an ensemble of independent, large spins. At low temperatures the intramolecular exchange constants J_{ij} are large compared to $k_B T$, so S will take a unique value. We describe a spin state by the quantum numbers S and m (the eigenvalue of $\hat{S}_z$).

A subset of these materials have their zero-field $(2S+1)$-fold spin degeneracy lifted by an anisotropy term in the Hamiltonian given by $D\hat{S}_z^2$, with $D < 0$. This will create an anisotropy energy barrier, and force the highest spin eigenvalue $m = \pm S$ to be the ground state of the

system. These materials are known as single-molecule magnets (SMMs) [25–27]. The highest energy state will be $m = 0$ (for integer S) or $m = 1/2$ (for half-integer S). The energy barrier is defined as $U_{\rm barrier} = |D|S^2$ for integer spins and $U_{\rm barrier} = |D|(S^2 - 1/4)$ for half-integer spins.

In the presence of a magnetic field $\mathbf{B}$, the simplest Hamiltonian $\hat{H}_{\rm e}$ describing SMMs at low temperatures is

$$\hat{H}_{\rm e} = D\hat{S}_z^2 + g\mu_{\rm B}\hat{\mathbf{S}} \cdot \mathbf{B}, \tag{4}$$

where the system is assumed to be axially symmetric and higher order fine structure terms are neglected. Saturation of the magnetization may be achieved via the application of the magnetic field along z (which defines the easy axis for the HSM), resulting in the unique ground state $m = -S$, with the highest energy state $m = 0$ (for integral S) or $m = 1/2$ (for half-integral S). Removal of the field results in a relaxation toward equilibrium requiring a fraction of spins to increase their value towards the higher energy state $m = 0$ or $1/2$, before decreasing their energy by further increasing their spin towards $m = +S$.

At elevated temperatures, dynamical spin processes may involve thermal excitation over the anisotropy barrier. At lower temperatures, however, the system must tunnel through the barrier. The possibility of an inherently quantum mechanical mechanism (quantum tunnelling) being directly detectable makes these systems attractive for both theoretical and experimental study.

One consequence of the Hamiltonian in equation (4) is that states $|m = l\rangle$ and $|m = -n\rangle$, where $l, n > 0$ (i.e. states on opposite side of the anisotropy barrier), may be brought into resonance by tuning the magnetic field. The condition for this is that

$$B = \frac{(l - n)D}{g\mu_{\rm B}}. \tag{5}$$

The Hamiltonian given in equation (4) cannot, with the magnetic field directed along the z-axis, describe tunnelling between different spin states since it commutes with $\hat{S}_z$. In reality, the symmetry of the system may require the addition of non-commuting crystal field terms to the Hamiltonian, or an additional physical mechanism may contribute a non-commuting term, such as spin–phonon interactions [28], dipolar interactions and nuclear fluctuations [29]. With the inclusion of this non-commuting term we may observe tunnelling between states $|l\rangle$ and $|-n\rangle$, if the anisotropy barrier can be crossed.

Magnetization data on these systems illustrate this behaviour (see, for example, [30]). Temperature independent hysteresis is observed for fixed sweep rate $\mathrm{d}B/\mathrm{d}t$, with significant steps occurring for the fields given by equation (5). The steps are accompanied by a decrease in relaxation time for the magnetization at the same field as the system tunnels through the barrier.

In the following sections, we consider the theory of μ^+SR in high spin systems and present the results of muon spin relaxation measurements on several examples of high spin systems with differing values of S and D. We find behaviour consistent with previous μ^+SR studies on similar HSMs [31, 32], allowing us to identify trends in the μ^+SR data that characterize these systems.

4.2. Towards a theory of muon spin relaxation in single-molecule magnets

The expected results from μ^+SR measurements on an ensemble of HSMs may be calculated from quantum mechanical properties of the system [33]. The Hamiltonian for a muon with spin $\mathbf{I}$ in a magnetic field $\mathbf{B}$ interacting with an electronic spin $\mathbf{S}$ is

$$\hat{H} = \hat{H}_{\rm e} + g\mu_{\rm B}\hat{\mathbf{I}} \cdot \mathbf{B} + A\hat{\mathbf{I}} \cdot \hat{\mathbf{S}}, \tag{6}$$

where we have chosen, for simplicity, to consider only an isotropic interaction between the muon and electronic spin, with hyperfine constant A. We may write this as

$$\hat{H} = \hat{H}_0 + \hat{H}_\mathrm{I}, \tag{7}$$

where

$$\hat{H}_0 = \hat{H}_\mathrm{e} + g\mu_\mathrm{B}\hat{\mathbf{I}} \cdot \mathbf{B}, \tag{8}$$

where, in our experiments, the magnetic field is always directed along the muon spin polarization direction. The interaction Hamiltonian $\hat{H}_\mathrm{I}$ is given by $\hat{H}_\mathrm{I} = A\hat{\mathbf{I}} \cdot \hat{\mathbf{S}}$. Considering $\hat{H}_\mathrm{I}$ as a perturbation to $\hat{H}_0$ yields the relaxation rate λ [34] given by

$$\lambda = \frac{A^2}{2\hbar^2}\int_{-\infty}^{\infty}\langle \hat{S}_-(t)\hat{S}_+(0)\rangle \exp(\mathrm{i}\omega t)\,\mathrm{d}t, \tag{9}$$

where $\omega = \gamma_\mu B$. Expanding the Heisenberg operator $\hat{S}_-(t)\hat{S}_+(0)$ in terms of the eigenstates $|q\rangle$ of the unperturbed Hamiltonian in equation (8) (corresponding to energies E_q), we obtain the matrix elements

$$\begin{aligned}\langle a|\hat{S}_-(t)\hat{S}_+(0)|b\rangle = {} & \sum_{m_i=-S}^{S-1}\langle m_i|b\rangle(S(S+1) - m_i(m_i+1))^{\frac{1}{2}} \\ & \times \left\{\sum_{c=1}^{2S+1}\langle c|m_i+1\rangle \exp\left(\frac{\mathrm{i}E_c t}{\hbar}\right)\left[\sum_{m_k=-S+1}^{S}\langle m_k|c\rangle(S(S+1) - m_k(m_k-1))^{\frac{1}{2}}\right.\right. \\ & \left.\left. \times \langle a|m_k - 1\rangle \exp\left(\frac{-\mathrm{i}E_a t}{\hbar}\right)\right]\right\}. \end{aligned} \tag{10}$$

If we make the additional assumption of Lorentzian level broadening, we obtain the result

$$\begin{aligned}\lambda = {} & \frac{A^2}{2\hbar^2}\sum_{a=1}^{2S+1}\exp(-E_a\beta)\left(\sum_{m_i=-S}^{S-1}\langle m_i|b\rangle(S(S+1) - m_i(m_i+1))^{\frac{1}{2}}\right. \\ & \times \left\{\sum_{c=1}^{2S+1}\langle c|m_i+1\rangle\left(\frac{\tau_c}{1+\omega'^2\tau_c^2}\right)\right. \\ & \left.\left. \times \left[\sum_{m_k=-S+1}^{S}\langle m_k|c\rangle(S(S+1) - m_k(m_k-1))^{\frac{1}{2}}\langle a|m_k-1\rangle\right]\right\}\right), \end{aligned} \tag{11}$$

where $\beta = 1/k_\mathrm{B}T$, τ_i is the lifetime of the ith level and

$$\omega' = \omega + \frac{E_\mathrm{c} - E_\mathrm{a}}{\hbar}. \tag{12}$$

In order to calculate the expected behaviour of the spin relaxation, the Hamiltonian in equation (8) was diagonalized numerically for a given value of S and given magnitude and direction of $\mathbf{B}$ and the resulting eigenvalues and amplitudes substituted in equation (11). We consider the case where the system may be rotated such that the magnetic field makes an angle θ with the z-axis of the SMM.

The main features of the theory may be illustrated in the simple case of a $S = 2$ system. Setting the parameters to be $D = -0.07$ K, $A = 100$ MHz, $T = 10$ K and $\tau_i = 0.1$ ns for all i, we obtain the results shown in figure 7. With the magnetic field directed along the z direction ($\theta = 0°$) the energy levels, calculated from the Hamiltonian in equation (4), show crossings at the magnetic fields predicted by equation (5). The corresponding relaxation rate λ shows peaks at the crossings for which $\Delta m = \pm 1$. The relaxation rate is seen to vanish at high fields. As expected, the peaks may be made sharper by increasing the lifetime of the

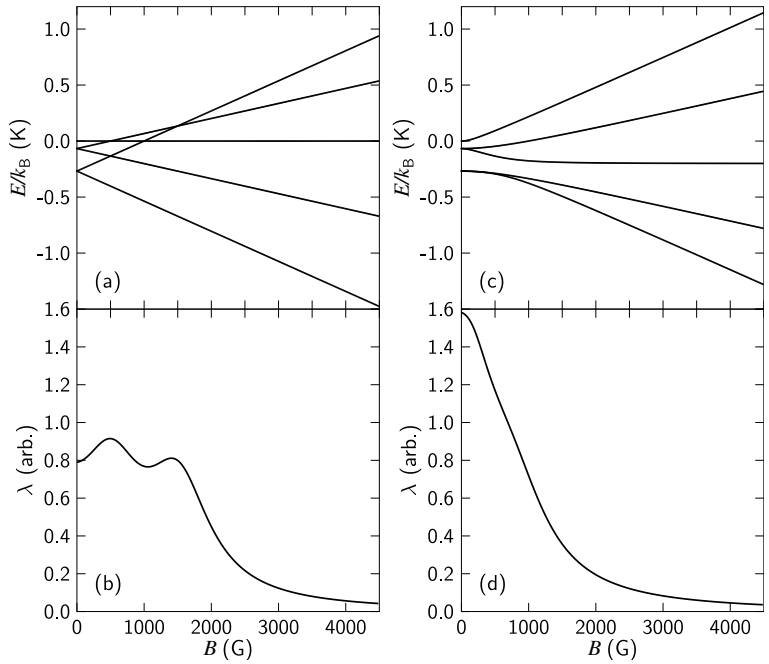

Figure 7. Calculated energy levels and relaxation rates for $S = 2$, $D = -0.07$ K, $A = 100$ MHz and $T = 10$ K. (a) Expected energy levels from equation (4) as a function of B along the z direction ($\theta = 0°$). The energy levels cross at values predicted by equation (5). (b) The calculated relaxation rate for $\theta = 0°$ with other parameters as described in the text. (c) Expected energy levels as a function of B perpendicular to the z direction ($\theta = 90°$). (d) The relaxation rate for $\theta = 90°$ with other parameters as described in the text.

levels. Significantly different results are obtained when **B** is perpendicular to the easy axis of the SMM ($\theta = 90°$). The energy levels are no longer observed to cross at the fields given by equation (5) and the relaxation rate λ is considerably larger in magnitude at low fields with no clear features observable near the peaks observed for the $\theta = 0°$ case.

The evolution of the energy levels and relaxation rate with θ is shown in figure 8 for the case of $S = 4$ (all other parameters are the same as for the previous case). We see that the high field level crossings are extinguished first as θ is increased from $\theta = 0°$, with none observed for $\theta = 90°$. The relaxation rate λ increases sharply at low fields with increasing angle, with the peaks becoming less well defined before their eventual disappearance.

All of the measurements reported here were made on samples in polycrystalline form (i.e. the easy axis (z-axis) of each crystallite makes a different angle θ to the applied magnetic field). We must therefore consider the case of a distribution in θ. As an example we consider the calculated value of λ as a function of angle at a field of 2000 G, as shown in figure 9(a). For a distribution in which each angle has an equal probability of occurring, the probability density of the relaxation rate $p(\lambda)$ is shown in figure 9(b). This function is peaked at the values of λ for which $\mathrm{d}\lambda/\mathrm{d}\theta$ is smallest in figure 9(a). The probability of an angle θ being realized should include a weighting factor $\sin\theta$, reflecting the available phase space for that particular θ. The inclusion of this factor results in the probability distribution seen in figure 9(c). The statistical weight close to 0° is reduced as there is little available phase space for these angles. This is reflected in a reduction of the peak in the probability density around the values of λ corresponding to 0°. The low λ peak corresponding to angles around 90° is, of course, barely

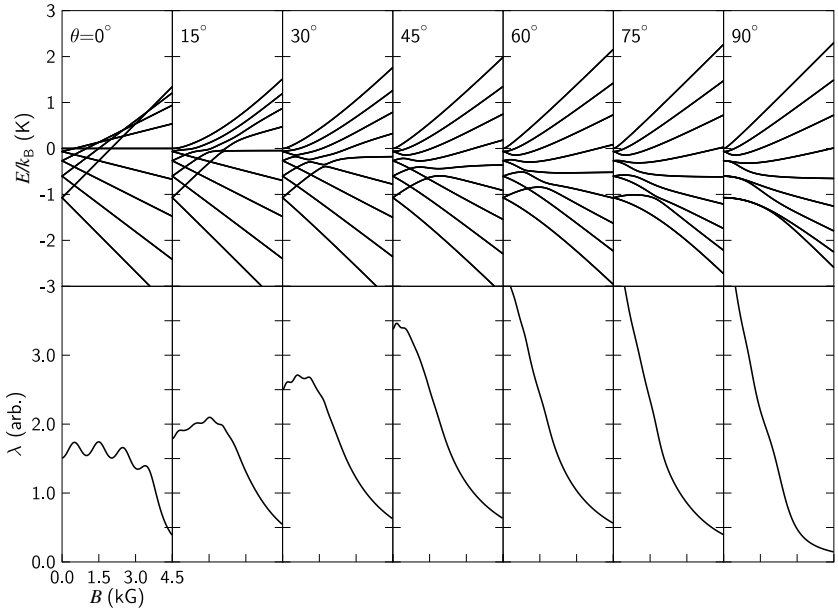

Figure 8. The evolution of the energy levels and relaxation rate λ with angle θ for a $S = 4$ system (all x-axes have the same scale). The peaks observed for the $\theta = 0$ case become less well defined as θ is increased. As θ increases from 0°, the relaxation rate increases at low fields.

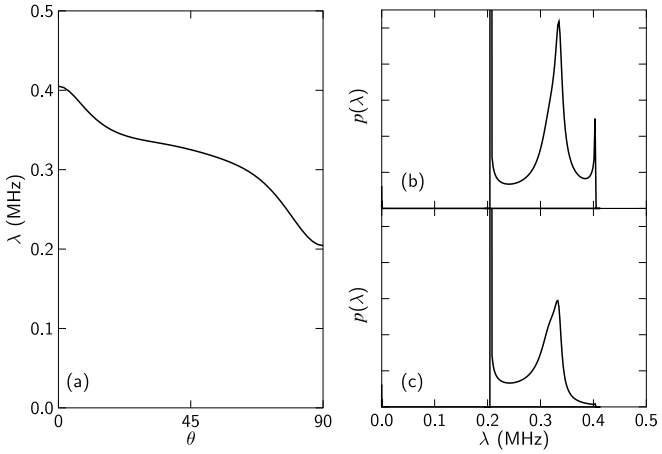

Figure 9. Angle dependent behaviour of a $S = 2$ system in an applied field of $B = 2000$ G. (a) The relaxation rate λ as a function of angle θ. (b) The relaxation rate probability density $p(\lambda)$ against λ for a uniformly distributed range of angles. (c) The relaxation rate probability density $p(\lambda)$ against λ, when angles are weighted with the necessary $\sin\theta$ factor.

altered by the inclusion of this factor. It is clear from these results that polycrystalline averaging will have a significant effect on the experimentally measured spectra of these systems.

4.3. μ^+SR data

The applicability of the full theory to spectra measured on polycrystalline samples is limited by several factors. In complex molecular systems there is a strong possibility of multiple muon

sites. Strictly speaking, each spectrum must be fitted to a distribution of exponential relaxation rates λ for each muon site. There is also the possibility of other contributions to the measured relaxation not related to the high spin properties (e.g. contributions from nuclear moments). Another significant difficulty is that the temperature dependence of the level lifetimes τ_i is not known and cannot be modelled with a simple spin–phonon interaction (see below). We are prompted, therefore, to adopt a phenomenological approach to the analysis in this paper. Although this prevents us from directly relating the μ^+SR results to the quantum properties of the system, it does allow us to characterize the interaction of the muon with several HSM materials.

4.3.1. A cyclic dodecanuclear nickel SMM. The compound $[Ni_{12}(chp)_{12}(O_2CMe)_{12}(H_2O)_6(THF)_6]$ (where chp = 6-chloro-2-pyridonate; the compound is hereafter called Ni_{12}) is the first SMM based on nickel(II) centres. The molecular structure is cyclic, with twelve Ni(II) centres bridged by pyridonate and acetate ligands [35, 36] (see figure 10(b)). The Ni_{12} forms a crystalline structure with all rings packing parallel to each other, perpendicular to the crystallographic c-axis in the rhombohedral space group $R\bar{3}c$ and has a $S = 12$ ground state. Magnetization and susceptibility measurements provide a value of $D/k_B = -0.067$ K (corresponding to an effective energy barrier $U_{barrier}/k_B = 9.65$ K) [36].

Polycrystalline samples of Ni_{12} were produced as described in [35, 36]. ZF μ^+SR measurements were made on these samples on the MuSR beamline at ISIS, using a dilution refrigerator and a sorption cryostat. An example of the measured asymmetry spectra is shown in figure 10(a). Spectra were found to be best fitted using the form

$$A(t) = A_0 \exp(-\lambda t) + A_{bg} \exp(-\lambda_{bg} t). \tag{13}$$

The term $A_{bg} \exp(-\lambda_{bg} t)$ describes a background contribution from a number of possible muon stopping states, including muons that stop in the sample holder or cryostat tail and from possible paramagnetic muon species in the crystal. A_0, A_{bg} and λ_{bg} were found to be constant across the measured temperature range. A single temperature dependent relaxation rate suggests a single muon site in this material.

An exponential decay of asymmetry is often characteristic of relaxation due to dynamic processes [17]. This interpretation is strengthened by the observation that applied magnetic fields as high as 4500 G do not decouple the relaxation.

The temperature dependence of λ is shown in figure 10(c). We see that as the temperature is decreased, the relaxation rate increases and then saturates at $T_{sat} \approx 2$ K. This behaviour is consistent with previous μ^+SR studies of HSMs [31, 32]. We might expect the temperature dependent part at $T > 2$ K to reflect thermal excitations of the system, which typically follow a temperature activated behaviour $\lambda \sim C \exp(V/T)$. We must also include the temperature independent term for low temperatures $\lambda \sim \lambda_0$. The relaxation rate in figure 10(c) is shown fitted to the resulting phenomenological form [31]:

$$\frac{1}{\lambda} = \frac{1}{\lambda_0} + \frac{1}{C \exp(V/T)}. \tag{14}$$

This yields parameters $1/\lambda_0 = 0.177(4)$ MHz^{-1}, $V = 13.4(4)$ K and $1/C = 5.6(3)$ MHz^{-1}.

Measurements were also made as a function of applied longitudinal B-field from 0 to 2400 G, and then from 2400 to 0 G. No hysteresis effects were discernible in the data. Equation (13) was again used to fit the data, with the term A_{bg} varying in an approximately linear fashion with applied field. The variation of this term may reflect the repolarization of paramagnetic muon states, or a shift in the experimental parameter α (discussed in section 2). The field dependence of λ at 4.2 K and 100 mK is shown in figure 10(d). At 4.2 K, we see

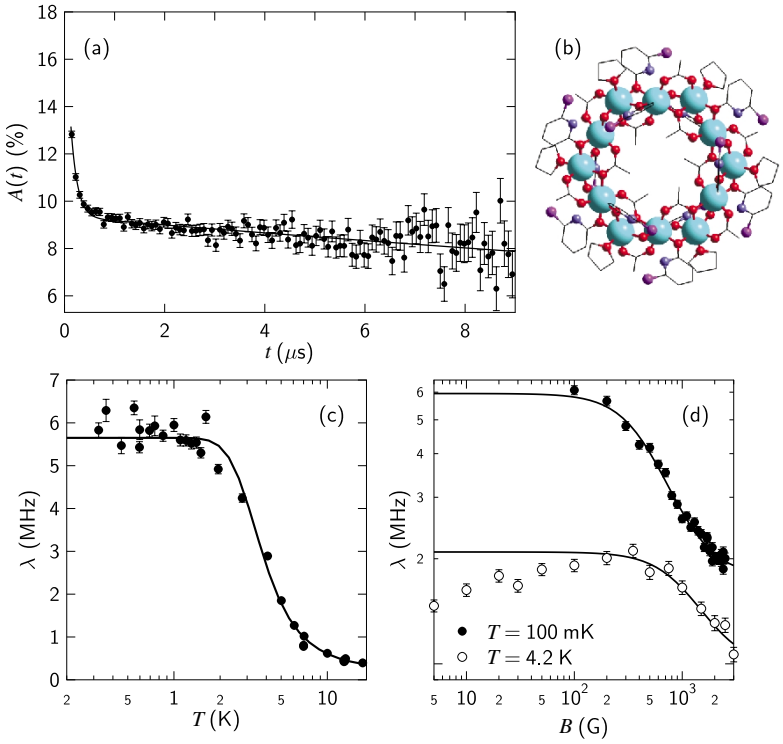

Figure 10. (a) The ZF spectrum for Ni_{12} measured at 500 mK. The solid curve is a fit to equation (13). (b) The molecular structure of $[Ni_{12}(chp)_{12}(O_2CMe)_{12}(H_2O)_6(THF)_6]$. (c) The temperature dependence of the relaxation rate λ in zero applied field. (d) The relaxation rate λ for Ni_{12} as a function of B-field at 4.2 K (open circles) and 100 mK (closed circles), after the application of B-fields as described in the text.

that at low fields the rate increases, with a maximum at $B \sim 300$ G, followed by a monotonic decrease at higher fields.

The observed field dependence may be attributed to the polycrystalline average of the functions considered in section 4.2. For the reasons outlined above, we choose to parametrize the field dependence with a simpler semi-phenomenological form [17, 31]:

$$\lambda = \frac{2\Delta^2\nu}{\omega^2 + \nu^2} + \lambda_{\text{offset}}, \tag{15}$$

where ν is the fluctuation rate, Δ is the field width and λ_{offset} is an offset from zero. A fit to equation (15) in the high field regime is shown in figure 10(d). The fitted parameters for $T = 4.2$ K are $\nu = 103(18)$ MHz, $\Delta/\gamma_\mu = 90(20)$ G and $\lambda_{\text{offset}} = 0.98(6)$ MHz, while at 350 mK we obtain $\nu = 46(1)$ MHz, $\Delta/\gamma_\mu = 115(4)$ mT and $\lambda_{\text{offset}} = 1.72(2)$ MHz.

4.3.2. An enneanuclear manganese cage. The compound $[Mn_9O_7(OAc)_{11}(thme)(py)_3(H_2O)_2]$ (hereafter Mn_9) consists of a $[Mn^{III}_4Mn^{II}_2O_6]^{4+}$ ring on which is placed a smaller $[Mn^{IV}_3O]^{10+}$ ring (see figure 11(b)). The material crystallizes in the monoclinic space group $P2_1/n$. The ground state of the molecule has $S = 17/2$ as a result of an antiferromagnetic interaction between the three ferromagnetically coupled Mn^{IV} ions and the wheel of four Mn^{III} and two Mn^{II} ions. Magnetization and susceptibility measurements provide a value of $D/k_B = -0.42$ K (corresponding to a barrier height of $U_{\text{barrier}}/k_B = 30.24$ K [37, 38]).

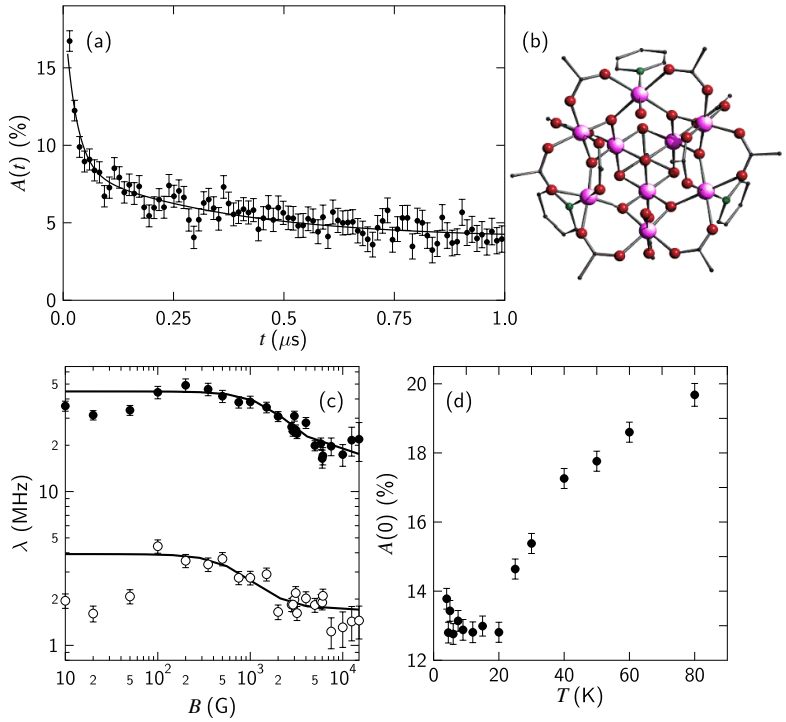

Figure 11. (a) A typical ZF spectrum for Mn_9 measured at 400 mK. The solid curve is a fit to equation (16). (b) The molecular structure of $[Mn_9O_7(OAc)_{11}(thme)(py)_3(H_2O)_2]$. (c) The behaviour of relaxation rates with applied magnetic fields. (d) The temperature dependence of the initial asymmetry from spectra measured at ISIS.

Powder samples of Mn_9 were synthesized as described in [38]. Measurements on Mn_9 were made on the LTF instrument at PSI. ZF measurements were made in the temperature range 0.02–1.1 K. There was little change in the spectra across this range suggesting that we are in a low temperature regime similar to that observed in Ni_{12} where λ is constant.

An example spectrum is shown in figure 11(a). Spectra were best fitted with an expression of the form

$$A(t) = A_1 \exp(-\lambda_1 t) + A_2 \exp(-\lambda_2 t) + A_{\rm bg}. \tag{16}$$

The presence of two separate field dependent relaxation rates suggests two distinct muon sites in this material. In the saturation regime, we obtain $\lambda_1 = 39(5)$ MHz, $\lambda_2 = 2.7(6)$ MHz and $A_1/A_2 = 2.9(5)$. To obtain the field dependent behaviour, A_1 and A_2 were fixed and $A_{\rm bg}$ allowed to vary with field for the reasons discussed in section 4.3.1. Since fields up to 15 000 G did not cause repolarization, we conclude that the observed relaxation is due to dynamic processes.

Figure 11(c) shows the behaviour of the two relaxation rates as a function of B-field at 20 mK. Again we note that the relaxation rates increase below 100 G, before their expected monotonic decrease at higher fields. Fitting the high field data to equation (15) yields, for λ_1, $\nu = 190(20)$ MHz, $\Delta/\gamma_\mu = 570(90)$ G and $\lambda_{\rm offset} = 17(1)$ MHz, while for λ_2, we obtain $\nu = 73(20)$ MHz, $\Delta/\gamma_\mu = 100(30)$ G and $\lambda_{\rm offset} = 1.7(1)$ MHz.

Data were also taken at ISIS on Mn_9 at temperatures up to 80 K. While the relaxation is too large (as compared with the ISIS time window) to fit with any confidence over most of the temperature range, we may extract the initial asymmetry $A(t = 0)$, as shown in figure 11(d).

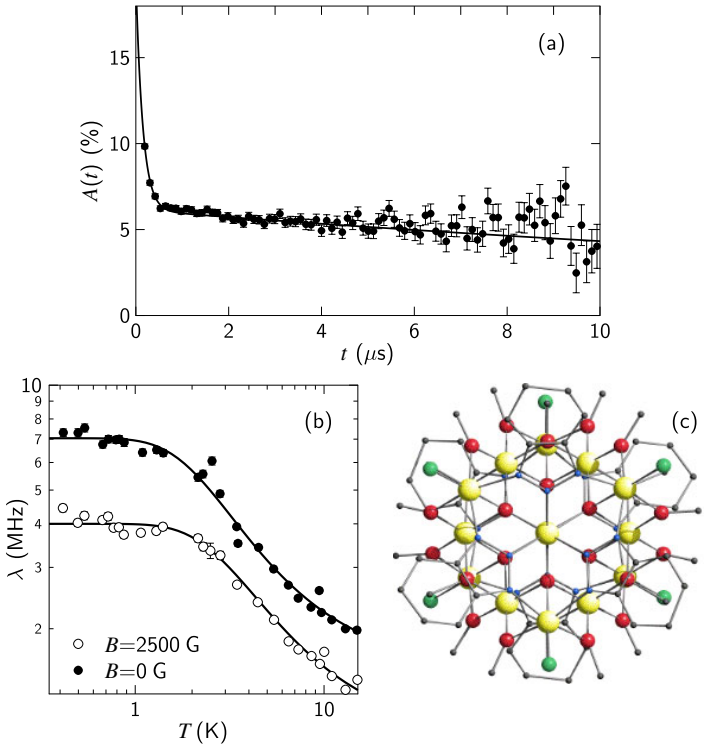

Figure 12. (a) The ZF spectrum for Fe_{14}, measured at 0.67 K. (b) The relaxation rate λ for Fe_{14} at $B = 0$ and 2500 G as a function of temperature. (c) The molecular structure of $[Fe_{14}(bta)_6O_6(OMe)_{18}Cl_6]$.

We observe an increase in initial asymmetry as temperature is increased corresponding to a reduction in relaxation rate due to temperature induced fluctuations. From the figure, we can infer that the saturation temperature is $1.1 \leqslant T_{sat} \leqslant 20$ K.

4.3.3. A tetradecametallic iron cluster. The compound $[Fe_{14}(bta)_6(O)_6(OMe)_{18}Cl_6]$ (hereafter Fe_{14}), where bta = benzotriazole, is a hexacapped hexagonal bipyramid with the caps on alternate faces [39] (see figure 12(c)). It is the first example of an Fe_{14} cluster. Magnetization measurements [39] suggest an $S \geqslant 23$ ground state with $D \approx 0.12$ K. This material is not, therefore, a SMM, since the positive value of D favours an $m = 0$ ground state.

Measurements were made on a powder sample of Fe_{14} (synthesized as described in [39]) using a sorption cryostat on the MuSR beamline at ISIS. An example spectrum, measured at 0.67 K, is shown in figure 12(a). Applied LF fields suggest that the relaxation is dynamic across the measured temperature range. The measured spectra were fitted to the functional form of equation (13) with A_0, λ_{bg} and A_{bg} fixed across the temperature range.

The temperature dependence of the relaxation rate is shown in figure 12(b) for zero field and a field of 2500 G. As with μ^+SR measurements on Ni_{12} and on Fe_{19} [32] the general trend is an increase in the relaxation rate with decreasing temperature, with the rate (roughly) saturating below $T_{sat} \approx 2$ K. Fitting to equation (14) yields $V = 5.5(3)$ K, $1/C = 1.8(1)$ MHz^{-1} and $1/\lambda_0 = 0.142(3)$ MHz^{-1} at $B = 0$ G and gives $V = 7.1(6)$ K, $1/C = 1.2(1)$ MHz^{-1} and $1/\lambda_0 = 0.25(6)$ MHz^{-1} for $B = 2500$ G.

Table 1. Summary of the temperature dependent behaviour probed using ZF μ^+SR and fitted to equation (14).

Material	S	D (K)	$U_{\rm barrier}$ (K)	V (K)	$1/\lambda_0$ (MHz^{-1})	$1/C$ (MHz^{-1})
$CrNi_6$ [31]	15/2	0	0	63(2)	∼0.15	86(12)
$CrMn_6$ [31]	27/2	0	0	73(7)	∼0.05	1.5(4)
Fe_{19} [32]	31/2	−0.05	15.7	74(4)	0.050(3)	3.5(5)
Ni_{12}	12	−0.067	9.65	13.4(4)	0.177(4)	5.6(3)
Fe_{14}	⩾23	0.115	⩾60.8	5.5(3)	0.142(3)	1.8(1)

Table 2. Summary of the low temperature (i.e. $T < T_{\rm sat}$) dynamic behaviour probed using LF μ^+SR and fitted to equation (15).

Material	S	D (K)	ν (MHz)	Δ/γ_μ (G)
$CrNi_6$ [31]	15/2	0	100(10)	214(4)
$CrMn_6$ [31]	27/2	0	120(30)	389(21)
Fe_{19} [32]	31/2	−0.05	114(6)	390(10)
Ni_{12}	12	−0.067	46(1)	115(4)
$Mn_9(\lambda_1)$	17/2	−0.42	190(20)	570(90)
$Mn_9(\lambda_2)$	17/2	−0.42	73(20)	100(30)

4.3.4. Discussion. Table 1 summarizes the temperature dependent behaviour of high spin systems studied with μ^+SR and fitted with equation (14) (including those considered here along with previous studies [31, 32]). Table 2 summarizes the information extracted from LF μ^+SR using equation (15). In all cases considered in tables 1 and 2, the relaxation processes are dynamic down to dilution refrigerator temperatures. This has been demonstrated through the application of longitudinal magnetic fields as described above.

In zero applied field, the temperature dependence of the relaxation rate is characterized by a temperature independent part at $T < T_{\rm sat}$ and a monotonic decrease at higher temperatures, which may be described by a temperature activated relaxation rate. In Ni_{12} and Fe_{14}, $T_{\rm sat}$ occurs at ∼2 K, whereas in $CrNi_6$, $CrMn_6$ [31] and Fe_{19} [32] it occurs at ∼10 K. When fitted to equation (14), the activation temperature parameter V shows no correlation with $U_{\rm barrier}$, the anisotropy energy barrier. The observed behaviour, therefore, is unlikely to be due to fluctuations caused by excitations of the HSM system over the energy barrier. The presence of a temperature independent component at low temperatures prevents modelling of the level lifetimes in equation (11) in terms of a simple spin–phonon interaction [33, 28], making a complete quantum mechanical description of these results problematic.

The magnetic field dependent behaviour allows the extraction of parameters relating to fluctuation rates and field widths. Again, no obvious correlations between these parameters and the parameters from the Hamiltonian in equation (4) present themselves. The failure of the phenomenological functional form in equation (15) to describe the low field data may be attributable to polycrystalline averaging effects discussed in section 4.2. There is also the complication of a possible contributions to the relaxation from static nuclear moments and multiple muon sites. We are unable, therefore, to unambiguously account for this feature at present.

No enhancement of the relaxation rate λ is observed at the level crossings given by equation (5). This is probably to be expected, since the samples measured were in polycrystalline form and, as seen in section 4.2, the direction of the easy axis of a HSM with respect to the applied magnetic field is highly significant in determining the measured relaxation. Any features in λ for a particular orientation are likely to be unresolvable once combined with the signal from each of the other crystallites at different orientations.

Each data point in, for example, figures 10(c) or (d) results from a muon spectrum recorded over ∼20 min, at fixed field, whereas steps in the magnetization are only observed for a constant sweep rate, in the case of Ni_{12} for example, of >20 G s^{-1} [36].

In order to relate the μ^+SR results to the quantum properties of the HSM system, large single-crystal samples are highly desirable. The significant complication of polycrystalline averaging is then eliminated, allowing the measurement of the angle dependence of the relaxation rate λ. Samples of this kind will be measured in the near future.

5. Conclusions

We have made μ^+SR measurements on quasi-1D Cu-based chain compounds $CuX_2(pyz)$ (where X = Br, Cl, NCS). In both $CuBr_2(pyz\text{-}d_4)$ and $CuCl_2(pyz)$, oscillations in the asymmetry characteristic of a quasistatic magnetic field at two distinct muon sites provide evidence of a magnetically ordered phase below $T_N = 3.6(1)$ K for $CuBr_2(pyz\text{-}d_4)$ and $T_N = 3.2(2)$ K for $CuCl_2(pyz)$. In contrast, $Cu(NCS)_2(pyz)$ shows no evidence of a magnetic phase transition down to 0.35 K. In the halide materials, the Cu–halide–Cu chains are subject to the dominant exchange interaction while the Cu–(pyz)–Cu exchange is smaller. The situation is reversed for $Cu(NCS)_2(pyz)$.

A theoretical approach to the μ^+SR of HSMs shows that an enhancement of the measured relaxation is expected at the energy level crossings of the system. It predicts a strong dependence on the angle between the applied magnetic field and the easy axis of the HSM.

Measurements have been made on the HSM systems Ni_{12} ($S = 12$), Mn_9 ($S = 17/2$) and Fe_{14} ($S \geqslant 23$). Spectra measured in applied longitudinal magnetic fields at dilution refrigerator temperatures strongly suggest that dynamic local field fluctuations are responsible for the relaxation of the muon spin ensemble. The relaxation rate is seen to increase with decreasing temperature, saturating below a temperature T_{sat} and LF measurements allow a parametrization of fluctuation rates in these materials. No correlation between the extracted parameters and the quantum mechanical parameters S and D is found. Future work will include measurements on large single-crystal HSM samples where the complication of polycrystalline averaging is eliminated. This should allow a direct comparison with the theoretical results of section 4.2. It is hoped that these single-crystal samples will allow the quantum properties of these systems to be more effectively probed with the muon.

Acknowledgments

Part of this work was performed at the Swiss Muon Source, Paul Scherrer Institute, Villigen, Switzerland, and at the ISIS muon source, RAL, UK. We are grateful to Chris Baines at PSI and to the staff at ISIS for technical assistance. We thanks W Hayes for useful discussions. This work is funded by the EPSRC and by the EC-TMR Network 'Molecules as Nanomagnets' (HPRN-CT-1999-00012).

References

[1] Blundell S J *Magnetism: Molecules to Materials* ed J S Miller and M Drillon (New York: Wiley–VCH) pp 235–56
[2] Amato A 1997 *Rev. Mod. Phys.* **69** 1119
[3] Blundell S J, Husmann A, Jestadt T, Pratt F L, Marshall I M, Lovett B W, Kurmoo M, Sugano T and Hayes W 2000 *Physica* B **289** 115
[4] Lancaster T, Blundell S J, Pratt F L, Coronado E and Galan-Mascaros J R 2004 *J. Mater. Chem.* **14** 1518
[5] Lovett B W, Blundell S J, Pratt F L, Jestadt T, Hayes W, Tagaki S and Kurmoo M 2000 *Phys. Rev.* B **61** 12241
[6] Blundell S J, Steer C A, Pratt F L, Marshall I M and Letard J F 2004 *J. Phys. Chem. Solids* **65** 25

[7] Le L P, Keren A, Luke G M, Wu W D, Uemura Y J, Tamura M, Ishikawa M and Kinoshita M 1993 *Chem. Phys. Lett.* **206** 405
[8] Blundell S J, Pattenden P A, Pratt F L, Valladares R M, Sugano T and Hayes W 1995 *Europhys. Lett.* **31** 573
[9] Blundell S J, Pattenden P A, Valladares R M, Pratt F L, Sugano T and Hayes W 1994 *Solid State Commun.* **92** 569
[10] Lappas A, Prassides K, Vavekis K, Arcon D, Blinc R, Cevc P, Amato A, Feyerherm R, Gygax F N and Schenck A 1995 *Science* **267** 1799
[11] Ferlay S, Mallah T, Ouhab L, Veillet P and Verdaguer M 1995 *Nature* **378** 701
[12] Manson J L, Huang Q Z, Lynn J W, Koo H J, Whangbo M H, Bateman R, Otsuka T, Wada N, Argyriou D N and Miller J S 2001 *J. Am. Chem. Soc.* **123** 162
[13] Bordallo H N, Chapon L, Manson J L, Ling C D, Qualls J S, Hall D and Argyriou D N 2003 *Polyhedron* **22** 2045
[14] Manson J L 2004 in preparation
[15] King P J C, Cottrell S P, Lord J S, Scott C A and Kilcoyne S H 2000 *MuSR User Guide* http://www.isis.rl.ac.uk/muons/musr/mguide/index.htm
[16] Schenck A 1999 *Muon Science* ed S L Lee, S H Kilcoyne and R Cywinski (Bristol: Institute of Physics Publishing) p 39
[17] Hayano R S, Uemura Y J, Imazato J, Nishida N, Yamazaki T and Kubo R 1979 *Phys. Rev.* B **20** 850
[18] Uemura Y J, Yamazaki T, Harshman D R, Senba M and Ansaldo E J 1985 *Phys. Rev.* B **31** 546
[19] Matsuda M, Katsumata K, Kojima K M, Larkin M, Luke G M, Merrin J, Nachumi B, Uemura Y J, Eisaki H, Motoyama N, Uchida S and Shirane G 1997 *Phys. Rev.* B **55** 11953
[20] Schulz H J 1996 *Phys. Rev. Lett.* **13** 2790
[21] Bonner J C and Fisher M E 1964 *Phys. Rev.* **135** A640
[22] Duffy W Jr, Venneman J E, Strandburg D L and Richards P M 1974 *Phys. Rev.* B **9** 2220
[23] Hammar P R, Stone M B, Reich D H, Broholm C, Gibson P J, Turnbull M M, Landee C P and Oshikawa M 1999 *Phys. Rev.* B **59** 1008
[24] Chakhalian J A, Kiefl R F, Miller R, Brewer J, Dunsiger S R, Morris G, MacFarlane W A, Sonier J E, Eggert S, Affleck I, Keren A and Verdaguer M 2003 *Phys. Rev. Lett.* **91** 27202
[25] Wernsdorfer W 2001 *Adv. Chem. Phys.* **118** 99
[26] Christou G, Gatteschi D, Hendrickson D N and Sessoli R 2000 *Mater. Res. Soc. Bull.* **25** 66
[27] Winpenny R E P 2002 *J. Chem. Soc. Dalton Trans.* **1**
[28] Garg A 1998 *Phys. Rev. Lett.* **81** 1513
[29] Prokof'ev N V and Stamp P C E 1998 *Phys. Rev. Lett.* **80** 5794
[30] Wernsdorfer W, Ohm T, Sangregorio C, Sessoli R, Mailly D and Paulsen C 1999 *Phys. Rev. Lett.* **82** 3903
[31] Salman Z, Keren A, Mendels P, Scuiller A and Verdaguer M 2000 *Physica* B **289/290** 106
[32] Blundell S J, Pratt F L, Marshall I M, Steer C A, Hayes W, Letard J F, Heath S L, Caneschi A and Gatteschi D 2003 *Synth. Met.* **133/134** 531
[33] Salman Z 2002 *Preprint* cond-mat/0209497
Salman Z 2002 *PhD Thesis* Technion—Israel Institute of Technology, Haifa, Israel
[34] White R 1983 *Quantum Theory of Magnetism* (Berlin: Springer)
[35] Cadiou C, Murrie M, Paulsen C, Villar V, Wernsdorfer W and Winpenny R E P 2001 *Chem. Commun.* 2666
[36] Andres H, Basler R, Blake A J, Cadiou C, Chaboussant G, Grant C M, Gudel H U, Murrie M, Parsons S, Paulsen C, Semadini F, Villar V, Wernsdorfer W and Winpenny R E P 2002 *Chem. Eur. J.* **8** 4867
[37] Brechin E K, Soler M, Davidson J, Hendrickson D N, Parsons S and Christou G 2002 *Chem. Commun.* 2252
[38] Brechin E K, Soler M, Christou G, Davidson J, Hendrickson D N, Parsons S and Wernsdorfer W 2003 *Polyhedron* **22** 1771
[39] Low D M, Jones L F, Bell A, Brechin E K, Mallah T, Riviere E, Teat S J and McInnes E J L 2003 *Angew. Chem. Int. Edn Engl.* **42** 3781